


 Cite this: *RSC Adv.*, 2022, 12, 33479

# DLBLS\_SS: protein secondary structure prediction using deep learning and broad learning system

 Lu Yuan,  Xiaopei Hu, Yuming Ma\* and Yihui Liu\*

Protein secondary structure prediction (PSSP) is not only beneficial to the study of protein structure and function but also to the development of drugs. As a challenging task in computational biology, experimental methods for PSSP are time-consuming and expensive. In this paper, we propose a novel PSSP model DLBLS\_SS based on deep learning and broad learning system (BLS) to predict 3-state and 8-state secondary structure. We first use a bidirectional long short-term memory (BLSTM) network to extract global features in residue sequences. Then, our proposed SEBTCN based on temporal convolutional networks (TCN) and channel attention can capture bidirectional key long-range dependencies in sequences. We also use BLS to rapidly optimize fused features while further capturing local interactions between residues. We conduct extensive experiments on public test sets including CASP10, CASP11, CASP12, CASP13, CASP14 and CB513 to evaluate the performance of the model. Experimental results show that our model exhibits better 3-state and 8-state PSSP performance compared to five state-of-the-art models.

 Received 12th October 2022  
 Accepted 16th November 2022

DOI: 10.1039/d2ra06433b

[rsc.li/rsc-advances](http://rsc.li/rsc-advances)

## 1 Introduction

As an important part of cell composition, proteins are not only the basis of life activities, but also play an important role in transporting substances, catalyzing chemical reactions and immune functions. The tertiary structure of a protein determines its function. However, existing techniques for predicting tertiary structure are time-consuming and expensive.<sup>1,2</sup> Secondary structure is the spatial arrangement of atoms in the backbone of a peptide chain. The tertiary structure is formed by further folding on the basis of the secondary structure. Therefore, the study of protein secondary structure directly affects the prediction of tertiary structure.<sup>3,4</sup> As an important task in bioinformatics, protein secondary structure prediction (PSSP) not only contributes to the study of protein function and structure but also facilitates the design and development of new drugs.

According to the division method of the DSSP program, the 8 states of protein secondary structure include G (helix), I ( $\pi$ -helix), H ( $\alpha$ -helix), B ( $\beta$ -bridge), E ( $\beta$ -sheet), T (turn), S (bend) and C (coil).<sup>5</sup> The 8-state protein secondary structure can also be classified into 3 states: H (helix), B (strand) and C (coil).<sup>6,7</sup> In the early stages of research, machine learning methods such as support vector machines,<sup>8,9</sup> K-nearest neighbors,<sup>10,11</sup> and neural networks<sup>12,13</sup> focused extensively on 3-state PSSP. However, the complex 8-state secondary structure has richer protein information and is more conducive to protein research.

In recent years, continuously developed and improved deep learning techniques have been widely used in PSSP, which exhibit superior performance and can improve computing speed. The PSIPRED<sup>14</sup> method utilized two feedforward neural networks for PSSP. The JPred4 (ref. 15) method utilized the JNet algorithm to predict the secondary structure. The SSpro<sup>16</sup> model used an ensemble of BRNN for prediction. The DeepCNF<sup>17</sup> model utilized shallow neural networks and conditional neural fields to model the mapping relationship between features and labels. Zhou *et al.* introduced a convolutional architecture in a supervised generative stochastic network to improve PSSP.<sup>18</sup> The SSREDNs<sup>3</sup> model used deep recurrent encoder-decoder networks for PSSP. The SPIDER3 server utilized a deep model LSTM-BRNN for 3-state prediction.<sup>19</sup> The SPOT-1D method utilized an ensemble model consisting of LSTM-BRNN and residual network for prediction.<sup>20</sup> The NrtSurfP-2.0 model utilized CNN and BLSTM to extract local and global dependencies between amino acid residues.<sup>21</sup> The SAINT method introduced a self-attention mechanism in the Deep3I network to extract secondary structure features.<sup>22</sup> The OPUS-TASS method combined CNN, BLSTM and Transformer architectures to improve accuracy.<sup>23</sup> The MLPRNN method used two MLP blocks and one BGRU to predict the secondary structure.<sup>24</sup>

Inspired by the application and effectiveness of deep learning in PSSP, we propose SETCN to extract key deep features in protein sequences by introducing Squeeze-and-Excitation<sup>25</sup> (SE) blocks in temporal convolutional networks<sup>26</sup> (TCN). Since secondary structure recognition is affected by residues in front and rear positions, we further propose SEBTCN to extract deep features bidirectionally.

School of Computer Science and Technology, Qilu University of Technology (Shandong Academy of Sciences), Jinan 250353, China. E-mail: [mym@qlu.edu.cn](mailto:mym@qlu.edu.cn); [yxl@qlu.edu.cn](mailto:yxl@qlu.edu.cn)



To improve PSSP, we propose a novel prediction model DLBLS\_SS for 3-state and 8-state PSSP based on bidirectional long short-term memory<sup>27</sup> (BLSTM) network, SEBTCN and broad learning system<sup>28</sup> (BLS). The input features of the model are position-specific scoring matrix (PSSM)<sup>29</sup> profiles and one-hot encoding. In DLBLS\_SS, BLSTM can extract global interactions in residue sequences, SEBTCN can capture bidirectional key long-range dependencies between residues, and BLS can further quickly extract local optimal features and complete classification.

The main contributions of this paper include: (1) we propose SETCN by introducing the channel attention mechanism SE block in TCN, which can extract key deep features in the sequence. (2) We further propose SEBTCN by improving SETCN, which can bidirectionally extract key deep features in sequences. (3) We propose a novel PSSP model using BLSTM, SETCN and BLS to improve feature extraction of residue sequences. To the best of our knowledge, this is the first application of BLS in PSSP. (4) Experimental results on seven benchmark datasets demonstrate that the proposed method achieves state-of-the-art performance compared to five popular methods.

## 2 Material and methods

### 2.1. Bidirectional long short-term memory networks (BLSTM)

For long protein sequences, recurrent neural networks<sup>30</sup> not only have inevitable error accumulation when transmitting useful information, but also may have problems such as exploding gradients. Therefore, we use BLSTM to capture the global features of the sequence, which can extract important information while automatically discarding useless information. As shown in Fig. 1, BLSTM contains forward LSTM and backward LSTM, which can obtain bidirectional interactions of sequences through forward and backward extraction of information. The computation of a standard LSTM<sup>31</sup> cell at time  $t$  is as follows:

$$i_t = \sigma(W_{x_i} \times x_t + W_{h_i} \times h_{t-1} + b_i) \quad (1)$$

$$f_t = \sigma(W_{x_f} \times x_t + W_{h_f} \times h_{t-1} + b_f) \quad (2)$$

$$o_t = \sigma(W_{x_o} \times x_t + W_{h_o} \times h_{t-1} + b_o) \quad (3)$$

$$c_t = f_t \odot c_{t-1} + i_t \odot \tanh(W_{x_c} \times x_t + W_{h_c} \times h_{t-1} + b_c) \quad (4)$$

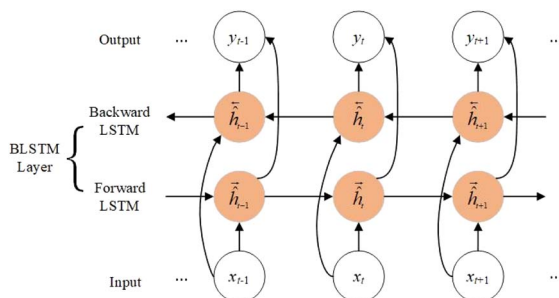


Fig. 1 The architecture of BLSTM.

$$h_t = o_t \odot \tanh(c_t) \quad (5)$$

where  $i$  is the input gate,  $f$  is the forget gate,  $o$  is the output gate,  $\sigma$  is the activation function,  $x_t$  is the input,  $h_t$  is the output,  $W$  is the weight,  $b$  is the bias,  $c_t$  is the unit state,  $\odot$  represents the element-wise multiplication, and  $\tanh$  represents the hyperbolic tangent function.

### 2.2. The proposed SEBTCN

As a sequence-to-sequence prediction network, TCN has the characteristics of stable training, low memory requirements, flexible receptive field, and parallel computing. To enhance the ability to extract key features in residue sequences, we introduce a channel attention module in the TCN residual block. Furthermore, secondary structure recognition is not only affected by residues in past positions, so we further propose SEBTCN to capture bidirectional deep features between residues.

**2.2.1. Dilated causal convolution.** The network uses causal convolution to prevent the loss of future information, so the output at time  $t$  depends on the input at time  $t$  and historical time. However, for sequences that rely on long histories, the network requires extremely deep architectures or large filters, which brings huge computational workload.

To expand the receptive field to obtain long historical information, the network introduces dilated convolutions. The computation of the dilated convolution  $F$  on the sequence element  $s$  is:

$$F(s) = (x \times df)(s) = \sum_{i=0}^{k-1} f(i) \cdot x_{s-d \cdot i} \quad (6)$$

where  $x$  is the input,  $f$  and  $k$  are the filter and filter size,  $d$  is the dilation factor, and  $s - d \cdot i$  is the history direction. Since the dilation factor increases exponentially with the number of layers in the network ( $d = 2^n$  at layer  $n$ ), the network has an extremely large receptive field and its top layers can get more information. The dilated causal convolution structure is shown in Fig. 2(a).

**2.2.2. Residual connections.** For high-dimensional sequences, the network may require extremely deep layers, but it is difficult to maintain stability during training. Therefore, as shown in Fig. 2(b), the network introduces residual connections, which operate on the input  $X$  as follows:

$$O = \text{activation}(X + F(X)) \quad (7)$$

where  $F$  is a series of transformations. Residual connections can allow each layer to learn to modify the identity map rather than all transformations, which is beneficial for very deep networks.

**2.2.3. SETCN residual block.** The architecture of the SETCN residual block is shown in Fig. 3. We utilize three dilated causal convolutional layers with the same dilation factor to extract features. After each layer of convolution, we also set an instance normalization layer to speed up network convergence, a ReLU layer to keep training stable, and a spatial dropout layer to avoid network overfitting. We add a channel attention module to



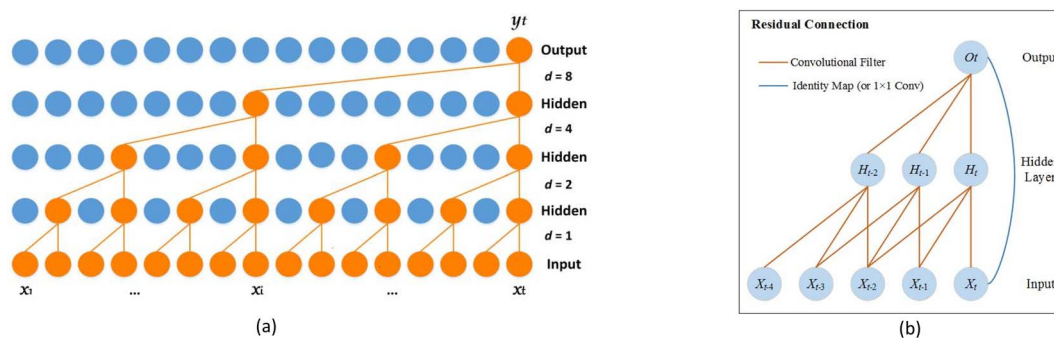


Fig. 2 Architecture in the network. (a) The dilated causal convolution. (b) The residual connection.

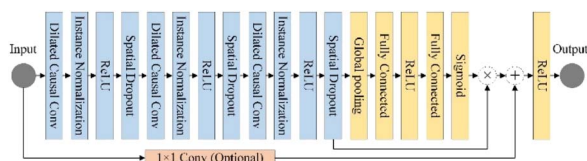


Fig. 3 The SETCN residual block.

extract key features after a series of convolutional transformations in the SETCN residual block. In channel attention, the global average pooling operation can compress the input features  $x \in R^{H \times W \times C}$  ( $H$  and  $W$  are the length and width of the input,  $C$  is the number of channels) into  $1 \times 1 \times C$ . Two fully connected layers are used for dimensionality reduction and restoration, respectively. We multiply the input of the channel attention with the weights normalized by the sigmoid function element-wise to obtain the output of the channel attention. Global average pooling of channel attention is defined as:

$$z_c = \text{ReLU}\left(\frac{1}{H \times W} \sum_{i=1}^H \sum_{j=1}^W x_c(i, j), 0\right) \quad (8)$$

The input of the SETCN residual block is added to the output of the channel attention, where  $1 \times 1$  convolution is used to ensure that the input and output have the same channels. Therefore, the output  $y_n = \text{ReLU}(f(W \times y_{n-1} + b) + y_{n-1})$  of the  $n$ th residual block.

**2.2.4. Architecture of SEBTCN.** Secondary structure prediction is not only influenced by past information but also related to future information. However, SETCN using dilated causal convolution does not rely on future features for sequence prediction. Therefore, we propose SEBTCN to extract bidirectional key features in sequences.

As shown in Fig. 4, the SEBTCN contains forward SETCN and backward SETCN. Let the protein sequence be  $X = \{x_1, x_2, \dots, x_L\}^{24}$  and the reverse sequence be  $X^{\leftarrow} = \{x_L, x_{L-1}, \dots, x_1\}$ , where  $L$  is the sequence length. SEBTCN can be calculated as:

$$\hat{Y} = \overrightarrow{\text{SETCN}}(X) \quad (9)$$

$$\hat{Y}_1 = \overleftarrow{\text{SETCN}}(\overleftarrow{X}) \quad (10)$$

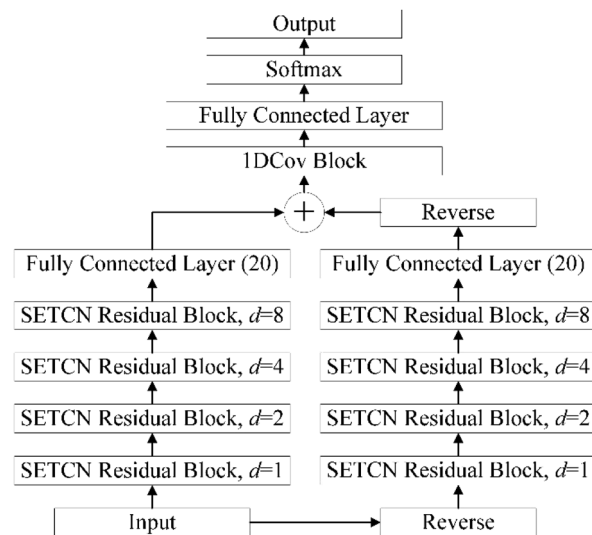


Fig. 4 The architecture of SEBTCN.

$$\text{Output} = \text{softmax}\left(F\left(\text{1DCov}\left(\hat{Y} \oplus \overleftarrow{\hat{Y}}_1\right)\right)\right) \quad (11)$$

where  $\hat{Y}$  and  $\hat{Y}_1$  represent the outputs of the forward and backward SETCN,  $\overrightarrow{\text{SETCN}}$  and  $\overleftarrow{\text{SETCN}}$  represent the forward and backward SETCN,  $\text{Output}$  represents the output of SEBTCN,  $\text{softmax}$  represents the activation function,  $F$  represents the operation of the fully connected layer, 1DCov represents operations such as convolution optimization of the 1DCov block,  $\overleftarrow{\hat{Y}}_1$  represents the reverse vector of  $\hat{Y}_1$ , and  $\oplus$  represents an element-wise addition operation.

Therefore, our SEBTCN can not only extract key feature information but also extract bidirectional deep dependencies. Furthermore, SEBTCN can be applied to all classification problems.

### 2.3. Broad learning system (BLS)

BLS is a flat network based on random vector functional-link neural networks,<sup>32</sup> which can effectively solve local optimal problems. As an efficient incremental learning system that does not require a deep network architecture, BLS has a simple



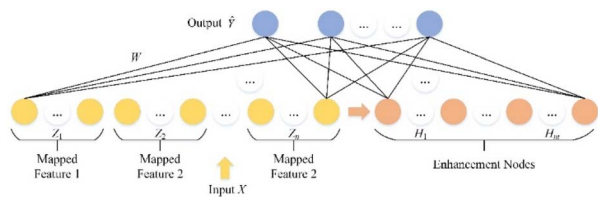


Fig. 5 The architecture of the BLS.

structure, an efficient modeling process, and can be updated dynamically and incrementally. As shown in Fig. 5, the architecture of BLS mainly consists of three parts: feature mapping layer, enhancement node layer and output layer. The network can randomly map input features to feature nodes. Then, the mapped features are expanded to the generated enhancement nodes. Finally, feature nodes and enhancement nodes are connected to the output.

Let the input feature matrix be  $X \in R^{N \times D}$ , and the secondary structure label be  $Y \in R^{N \times C}$ , where  $N$  is the number of samples,  $D$  is the sample dimension, and  $C$  is the number of categories. The mapping feature generated by the  $i$ th mapping feature node is:

$$Z_i = \phi(XW_{ei} + \beta_{ei}), i = 1, \dots, n \quad (12)$$

where  $\phi$  is the mapping function, and  $W$  and  $\beta$  are randomly generated weights and biases. To speed up the learning process during training, features are randomly mapped to enhancement nodes to improve nonlinear learning ability in feature extraction.

Let all feature nodes be  $Z^n \equiv [Z_1, Z_2, \dots, Z_n]$ , so the  $m$ th group of enhancement nodes can be calculated as:

$$H_m \equiv \xi(Z^n W_{hm} + \beta_{hm}) \quad (13)$$

where  $\xi$  is the activation function of the enhancement node. BLS can be calculated as follows:

$$Y = [Z_1, \dots, Z_n | H_1, \dots, H_m] W^m = [Z^n | H^m] W^m \quad (14)$$

where  $W^m = [Z^n | H^m]^+ Y$  is the output connection weight of BLS. Let  $A = [Z^n | H^m]$ , the network computes  $A^+$  by solving the ridge regression approximation:

$$A^+ = \lim_{\lambda \rightarrow 0} (\lambda I + AA^T)^{-1} A^T \quad (15)$$

#### 2.4. The proposed DLBLS\_SS

The detailed architecture of DLBLS\_SS is shown in Fig. 6. To improve PSSP, the proposed model combines deep learning and BLS to predict 3-state and 8-state secondary structure. DLBLS\_SS is mainly divided into four modules: input module, BLSTM feature extraction module, SEBTCN feature extraction module, BLS feature extraction and output module.

In the input module, we use the initial protein data to generate one-hot features and PSSM profiles. The input to the

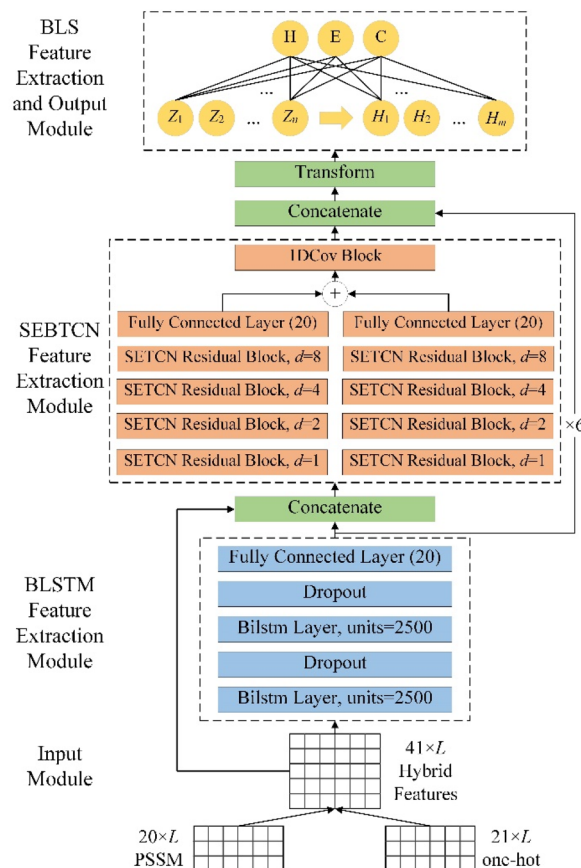


Fig. 6 The detailed architecture of DLBLS\_SS.

model is a  $41 \times L$  hybrid feature PSSM + one-hot, where  $L$  represents the residue length of the protein.

In the BLSTM feature extraction module, we use two BLSTM layers to extract global features in residue sequences. We also use a dropout layer after the BLSTM layer to avoid the risk of overfitting during training.

In SEBTCN feature extraction module, we fuse input features and global features extracted by BLSTM. We then use four SETCN residual blocks with channel attention to further bidirectionally capture key deep long-range dependencies between amino acid residues. Furthermore, a 1DCov block is used for fast optimization of features. The broad receptive field of SEBTCN can establish better long-range bidirectional interactions between sequence elements.

In the BLS feature extraction and output module, we first fuse the long-range features extracted by SEBTCN and BLSTM. Secondary structure prediction is mainly affected by local residues, so we use the sliding window technique to segment the fusion features into sequences of size  $40 \times 19$  and further transform them so that the model can extract local interactions. We use 40 feature node groups with 40 nodes to transform the input data into the mapping feature space. Then, the mapping features are expanded in a broad sense to 10 000 enhancement feature nodes for nonlinear learning. Finally, we obtain the output weights by computing the pseudo-inverse of the



mapping and enhancement features to complete the classification of the secondary structure.

The proposed model can not only capture key long-range interactions in protein sequences but also utilize local optimal features for 3-state and 8-state PSSP. Furthermore, the powerful feature extraction capability of our model can better model complex sequence–structure relationships between input sequences and structural labels.

## 3 Experiments

### 3.1. Datasets

The PISCES<sup>33</sup> server is widely used for PSSP, which can generate sequence subsets from the Protein Data Bank based on structural quality and mutual sequence identity. Therefore, we selected 14 991 proteins using the PISCES server with parameters including: the percent identity cutoff was set to 25%, the resolution cutoff was set to 3 Å, and the *R*-factor cutoff was set to 0.25. We removed sequences that were duplicated with the test set. In addition, proteins with sequence lengths less than 40 or more than 800 were also deleted. The final constructed CullPDB<sup>33</sup> dataset has 14 562 proteins. For testing purpose, we randomly divided the dataset into training set (11 650), validation set (1456) and test set (1456). We randomly divided the dataset three times for classification three times. The final prediction accuracy is the mean of the three prediction accuracy.

To evaluate the performance of the proposed model, we also use six public test sets CASP10,<sup>34</sup> CASP11,<sup>35</sup> CASP12,<sup>36</sup> CASP13,<sup>37</sup> CASP14 (ref. 38) and CB513,<sup>39</sup> where all CASP datasets are available at <https://predictioncenter.org/>. The statistics of the six datasets are shown in Table 1.

### 3.2. Features

In this work, we use two feature representation methods one-hot encoding and PSSM as the input to the model. Amino acids include 20 standard amino acids (A, C, D, E, F, G, H, I, K, L, M, N, P, Q, R, S, T, V, W, Y and X) and 6 non-standard amino acids such as B, X, and Z. Because the number of non-standard amino acids is low, they can be classified as one type. Therefore, we can consider that amino acids have 21 types. The one-hot encoding method can represent each type of amino acid as a 21-dimensional vector, in which the corresponding component of the amino acid is 1, and the remaining components are 0. Since the vectors of the 21 amino acid types are mutually orthogonal, one-hot encoding can also be called orthogonal encoding.

PSSM is a scoring matrix generated by aligning the sequence itself with multiple sequences, which is widely used for feature

representation. We use the PSI-BLAST<sup>40</sup> procedure to generate PSSM profiles, where the threshold *E* is set to 0.001 and the number of iterations is set to 3. PSSM can express an amino acid sequence of length *L* as an  $L \times 20$  feature matrix by scoring 20 standard amino acid types.

### 3.3. Evaluation metrics

In this work, to evaluate the overall prediction accuracy of the proposed model, we use four commonly used metrics:  $Q_3$  accuracy,  $Q_8$  accuracy and SOV<sup>41</sup> score for 3-state and 8-state PSSP. The secondary structure corresponding to the amino acid sequence was obtained by the DSSP5 program. Let the 3-state secondary structure  $S_3 = \{H, E, C\}$ , and the 8-state secondary structure  $S_8 = \{G, I, H, B, E, S, T, C\}$ .  $Q_3$  and  $Q_8$  overall accuracy is defined as:

$$Q_3(Q_8) = \frac{\sum n_s}{N} \times 100, \quad s \in S_3(s \in S_8) \quad (16)$$

where *N* is the total number of residues and  $n_s$  is the correct number of predicted type *s*. Let the total number of residues of the sequence be  $N_{SOV}$ , the observed segment be  $S_1$ , the predicted segment be  $S_2$ , and the overlapping segment of  $S_1$  and  $S_2$  be  $S_0$ . The SOV score can be calculated as follows:

$$SOV = \frac{100}{N_{SOV}} \sum_{S_0} \left[ \frac{\minov(S_1, S_2) + \sigma(S_1, S_2)}{\maxov(S_1, S_2)} \text{length}(S_1) \right] \quad (17)$$

where  $\maxov(S_1, S_2)$  and  $\minov(S_1, S_2)$  represent the union length and overlap length of the segments  $S_1$  and  $S_2$ , respectively. The  $\sigma(S_1, S_2)$  allowed to vary at the segment edges is calculated as:

$$\sigma(S_1, S_2) = \min \left\{ \begin{array}{l} \maxov(S_1, S_2) - \minov(S_1, S_2) \\ \minov(S_1, S_2) \\ \text{int}[\text{len}(S_1)]/2 \\ \text{int}[\text{len}(S_2)]/2 \end{array} \right\} \quad (18)$$

### 3.4. Performance analysis of the proposed model

In this section, to demonstrate the impact of the hyper-parameters of the three modules in DLBLS\_SS on the performance of 3-state and 8-state PSSP, we conduct extensive experiments using the CullPDB dataset.

**3.4.1. Influence of BLSTM module parameters.** To explore the effect of the number of units in the BLSTM layer on the proposed method, we conduct comparative experiments on the validation and test sets. We use two BLSTM layers, which is the best number demonstrated experimentally. As shown in Fig. 7, the model achieves the highest  $Q_3$  and  $Q_8$  accuracy on two datasets when using 2500 units. Because the number of units directly affects the ability to analyze high-dimensional residue sequences, too many hidden units can also lead to network overfitting.

**3.4.2. Influence of SEBTCN module parameters.** Since the number of SETCN residual blocks determines the receptive field of the model, we use different numbers of residual blocks to classify the validation and test sets. As shown in Fig. 8, the

Table 1 Number of proteins and residues in the six datasets

| Number   | CASP10 | CASP11 | CASP12 | CASP13 | CASP14 | CB513  |
|----------|--------|--------|--------|--------|--------|--------|
| Proteins | 99     | 81     | 19     | 22     | 23     | 513    |
| Residues | 24 048 | 20 084 | 4257   | 5948   | 4644   | 84 119 |



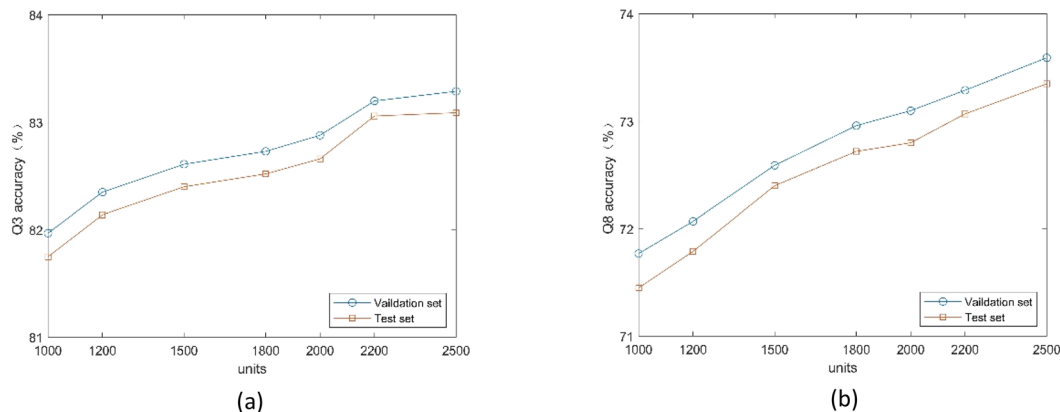


Fig. 7 (a)  $Q_3$  accuracy of the proposed method under different number of units. (b)  $Q_8$  accuracy of the proposed method under different number of units.

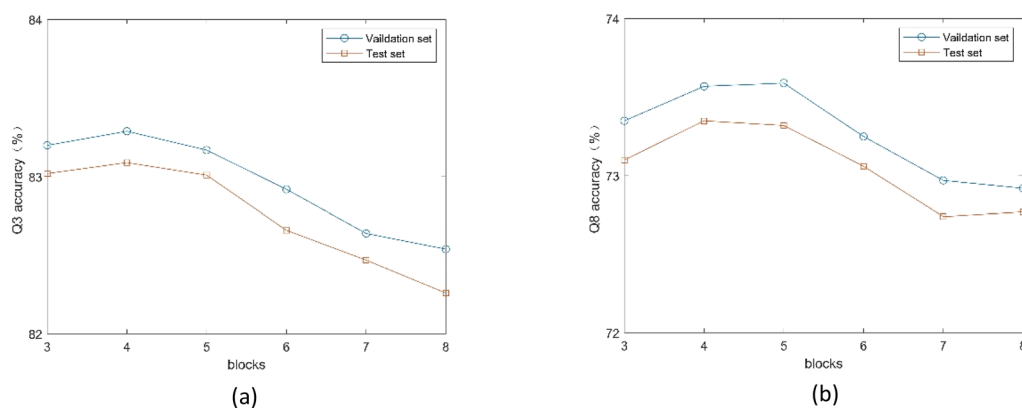


Fig. 8 (a)  $Q_3$  accuracy of the proposed method under different number of SETCN blocks. (b)  $Q_8$  accuracy of the proposed method under different number of SETCN blocks.

model achieves the best 3-state PSSP performance when the number of residual blocks is 4, and the model achieves the best 8-state PSSP performance on the two datasets when the number of residual blocks is 4 and 5, respectively. The main reason is that the number of residual blocks affects the depth of the

network. Also, too many residual blocks can trap the model in local optima.

**3.4.3. Influence of SEBTCN module parameters.** The number of feature nodes and enhancement nodes in the BLS module determines the network width. Fig. 9 shows the 3-state

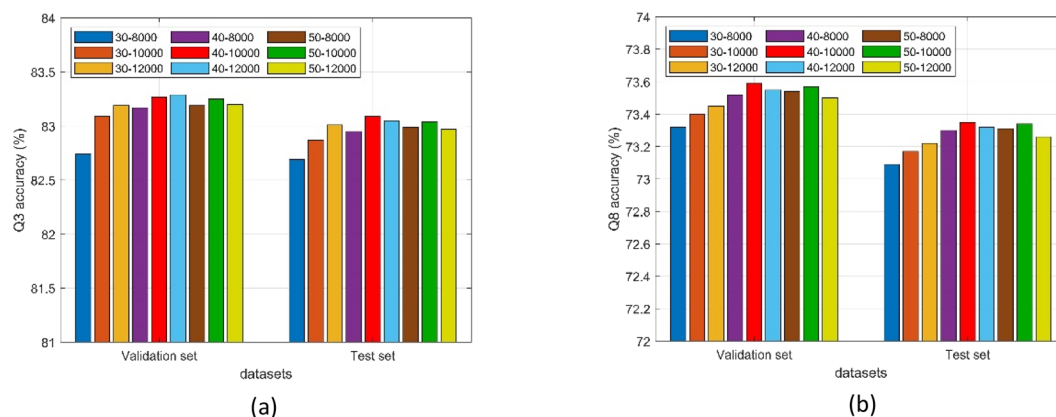


Fig. 9 (a)  $Q_3$  accuracy of the proposed method under different number of nodes. (b)  $Q_8$  accuracy of the proposed method under different number of nodes.



Table 2 3-state and 8-state PSSP results of six models on seven datasets. Bold indicates the best performance

| Models         | CullPDB        |                | CASP10         |                | CASP11         |                | CASP12         |                | CASP13         |                | CASP14         |                | CB513          |                |
|----------------|----------------|----------------|----------------|----------------|----------------|----------------|----------------|----------------|----------------|----------------|----------------|----------------|----------------|----------------|
|                | Q <sub>3</sub> | Q <sub>8</sub> | Q <sub>3</sub> | Q <sub>8</sub> | Q <sub>3</sub> | Q <sub>8</sub> | Q <sub>3</sub> | Q <sub>8</sub> | Q <sub>3</sub> | Q <sub>8</sub> | Q <sub>3</sub> | Q <sub>8</sub> | Q <sub>3</sub> | Q <sub>8</sub> |
| LSTM           | 74.05          | 62.87          | 75.66          | 65.47          | 74.68          | 63.22          | 74.67          | 62.98          | 73.91          | 61.68          | 73.55          | 62.77          | 76.87          | 66.87          |
| SETCN          | 75.62          | 64.79          | 77.79          | 66.95          | 75.73          | 64.89          | 76.14          | 64.85          | 74.96          | 63.01          | 74.69          | 63.85          | 80.11          | 68.12          |
| SEBTCN         | 81.39          | 70.92          | 82.75          | 71.79          | 80.96          | 70.07          | 80.57          | 69.97          | 80.91          | 67.96          | 80.54          | 69.39          | 84.82          | 73.94          |
| BLSTM          | 82.16          | 72.38          | 83.21          | 72.64          | 80.91          | 70.16          | 80.37          | 69.30          | 80.46          | 67.43          | 80.49          | 68.81          | 84.79          | 75.86          |
| BLSTM + SEBTCN | 82.97          | 73.22          | 83.73          | 73.54          | 81.60          | 71.52          | 81.14          | 70.39          | 81.27          | 68.41          | 81.18          | 69.97          | 85.74          | 77.06          |
| DLBLS_SS       | <b>83.10</b>   | <b>73.35</b>   | <b>84.06</b>   | <b>73.95</b>   | <b>81.76</b>   | <b>71.65</b>   | <b>81.28</b>   | <b>70.54</b>   | <b>81.39</b>   | <b>68.59</b>   | <b>81.32</b>   | <b>70.24</b>   | <b>85.90</b>   | <b>77.35</b>   |

and 8-state PSSP performance of the proposed method on validation and test sets under different numbers of nodes. The Q<sub>3</sub> accuracy of the model on the two datasets reaches the maximum when the feature nodes are 40 and the enhancement nodes are 10 000 and 12 000 respectively. The model achieves the highest Q<sub>8</sub> accuracy on two datasets when using 40 feature nodes and 10 000 enhancement nodes. Furthermore, the number of nodes not only determines the prediction performance but also affects the size of the model.

### 3.5. Ablation study

To demonstrate the effectiveness of the proposed models, we conduct comparative experiments with Q<sub>3</sub> accuracy and Q<sub>8</sub> accuracy as evaluation metrics. The comparison results of the six models on the seven datasets are shown in Table 2. Compared with SETCN, SEBTCN achieves an average improvement of 5.27% and 5.37% in Q<sub>3</sub> accuracy and Q<sub>8</sub> accuracy on seven datasets, which indicates that the proposed SEBTCN can sufficiently extract bidirectional key features in sequences. SETCN consistently outperforms LSTM in PSSP, while SEBTCN outperforms BLSTM in most cases, mainly because SEBTCN has a broad receptive field, but it also loses some important information. The integration of BLSTM and SEBTCN achieves higher 3-state and 8-state PSSP accuracy, which proves that SEBTCN can further extract long-range features. Furthermore, DLBLS\_SS achieves better prediction performance compared to BLSTM + SEBTCN, which proves that the introduction of BLS can effectively extract local features to improve classification accuracy.

As shown in Table 3, we compare the prediction performance of the proposed model under different input features on seven datasets. When the input is the hybrid feature PSSM + one-hot, the prediction accuracy of DLBLS\_SS reaches the maximum. Furthermore, it can be seen that PSSM features are significantly

better than one-hot features, mainly because PSSM contains richer biological information.

### 3.6. Comparison with popular models

In this section, we compare the proposed method with five state-of-the-art methods DCRNN,<sup>42</sup> CNN\_BIGRU,<sup>43</sup> DeepACLSTM,<sup>44</sup> MUFOLD-SS<sup>45</sup> and ShuffleNet\_SS<sup>46</sup> on seven test sets CullPDB, CASP10, CASP11, CASP12, CASP13, CASP14 and CB513. The DCRNN model utilizes a multi-scale convolutional neural network to extract local features and a bidirectional neural network composed of gated units to extract global features. The CNN\_BIGRU model utilizes convolutional networks and bidirectional gating units to improve the accuracy of PSSP. The DeepACLSTM model predicts secondary structure using local and long-range dependencies extracted by asymmetric convolutional and bidirectional long short-term memory networks. The MUFOLD-SS predictor utilizes the deep inception-inside-inception method for prediction. ShuffleNet\_SS introduces label distribution-aware margin loss in lightweight convolutional networks to improve rare class recognition. For the purpose of fair comparison, we use our dataset to train all models in the experiments, where the hybrid feature PSSM + one-hot is used as input.

To evaluate the prediction performance of the proposed model for 3-state and 8-state secondary structure, we employ Q<sub>3</sub> accuracy, Q<sub>8</sub> accuracy and SOV score as evaluation measures. The 3-state and 8-state PSSP comparison results of the proposed model and five existing popular models on seven benchmark datasets are shown in Tables 4 and 5. The comparison of Q<sub>3</sub> accuracy and SOV score in Table 4 shows that DLBLS\_SS exhibits better prediction performance in most cases compared to five popular methods. Table 5 shows that the 8-state PSSP performance of DLBLS\_SS consistently outperforms the five state-of-the-art models on the seven test sets. This is mainly

Table 3 Q<sub>3</sub> and Q<sub>8</sub> accuracy of DLBLS\_SS under different features on seven datasets. Bold indicates the best performance

| Features       | CullPDB        |                | CASP10         |                | CASP11         |                | CASP12         |                | CASP13         |                | CASP14         |                | CB513          |                |
|----------------|----------------|----------------|----------------|----------------|----------------|----------------|----------------|----------------|----------------|----------------|----------------|----------------|----------------|----------------|
|                | Q <sub>3</sub> | Q <sub>8</sub> | Q <sub>3</sub> | Q <sub>8</sub> | Q <sub>3</sub> | Q <sub>8</sub> | Q <sub>3</sub> | Q <sub>8</sub> | Q <sub>3</sub> | Q <sub>8</sub> | Q <sub>3</sub> | Q <sub>8</sub> | Q <sub>3</sub> | Q <sub>8</sub> |
| PSSM           | 82.08          | 72.13          | 82.96          | 72.71          | 80.63          | 70.37          | 80.13          | 69.28          | 80.22          | 67.31          | 80.17          | 68.95          | 84.74          | 76.05          |
| One-hot        | 72.74          | 62.79          | 73.59          | 63.18          | 72.27          | 61.97          | 72.79          | 62.01          | 71.92          | 59.57          | 72.41          | 61.21          | 75.02          | 65.97          |
| PSSM + one-hot | <b>83.10</b>   | <b>73.35</b>   | <b>84.06</b>   | <b>73.95</b>   | <b>81.76</b>   | <b>71.65</b>   | <b>81.28</b>   | <b>70.54</b>   | <b>81.39</b>   | <b>68.59</b>   | <b>81.32</b>   | <b>70.24</b>   | <b>85.90</b>   | <b>77.35</b>   |



Table 4 Performance comparison with state-of-the-art models on seven datasets in 3-state PSSP. Bold indicates the best performance

| Models        | CullPDB        |              | CASP10         |              | CASP11         |       | CASP12         |              | CASP13         |              | CASP14         |              | CB513          |              |
|---------------|----------------|--------------|----------------|--------------|----------------|-------|----------------|--------------|----------------|--------------|----------------|--------------|----------------|--------------|
|               | Q <sub>3</sub> | SOV          | Q <sub>3</sub> | SOV          | Q <sub>3</sub> | SOV   | Q <sub>3</sub> | SOV          | Q <sub>3</sub> | SOV          | Q <sub>3</sub> | SOV          | Q <sub>3</sub> | SOV          |
| DCRNN         | 82.12          | 78.51        | 82.57          | 75.71        | 80.57          | 75.53 | 80.41          | 74.75        | 80.49          | 77.09        | 80.27          | 71.46        | 84.65          | 79.63        |
| CNN_BIGRU     | 82.32          | 78.68        | 82.42          | 76.20        | 81.05          | 76.58 | 80.38          | 75.62        | 80.66          | 76.94        | 80.46          | 71.92        | 84.83          | 79.90        |
| DeepACLSTM    | 82.64          | 79.45        | 83.43          | 77.76        | 81.32          | 76.04 | 80.49          | 75.56        | 80.92          | 77.43        | 80.79          | 71.73        | 85.02          | 80.12        |
| MUFOLD-SS     | 83.02          | <b>79.62</b> | 83.28          | 78.04        | 81.67          | 77.41 | 80.92          | <b>77.47</b> | 81.15          | 78.02        | 81.13          | 70.97        | 85.30          | 80.23        |
| ShuffleNet_SS | 83.06          | 78.79        | 83.85          | 76.27        | 81.70          | 76.37 | 80.87          | 76.39        | <b>81.41</b>   | <b>77.46</b> | 81.24          | 71.32        | 85.61          | 79.98        |
| DLBLS_SS      | <b>83.10</b>   | 79.15        | <b>84.06</b>   | <b>78.13</b> | <b>81.76</b>   | 77.71 | <b>81.28</b>   | 75.98        | 81.39          | 77.18        | <b>81.32</b>   | <b>72.55</b> | <b>85.90</b>   | <b>80.67</b> |

Table 5 Performance comparison with state-of-the-art models on seven datasets in 8-state PSSP. Bold indicates the best performance

| Models        | CullPDB        |              | CASP10         |              | CASP11         |              | CASP12         |              | CASP13         |              | CASP14         |              | CB513          |              |
|---------------|----------------|--------------|----------------|--------------|----------------|--------------|----------------|--------------|----------------|--------------|----------------|--------------|----------------|--------------|
|               | Q <sub>8</sub> | SOV          | Q <sub>8</sub> | SOV          | Q <sub>8</sub> | SOV          | Q <sub>8</sub> | SOV          | Q <sub>8</sub> | SOV          | Q <sub>8</sub> | SOV          | Q <sub>8</sub> | SOV          |
| DCRNN         | 72.06          | 70.42        | 72.10          | 69.74        | 70.51          | 68.44        | 69.40          | 67.24        | 68.05          | 68.01        | 68.87          | 63.27        | 75.63          | 73.06        |
| CNN_BIGRU     | 72.30          | 70.15        | 71.89          | 69.17        | 70.95          | 69.05        | 69.68          | 68.06        | 67.84          | 67.92        | 68.69          | 62.95        | 75.55          | 72.84        |
| DeepACLSTM    | 72.87          | 71.34        | 73.08          | 71.42        | 71.24          | 69.93        | 69.82          | 68.18        | 68.46          | 69.31        | 69.55          | 63.46        | 76.02          | 73.46        |
| MUFOLD-SS     | 73.32          | 71.59        | 72.99          | 71.51        | 71.59          | 69.84        | 70.22          | 69.32        | 68.23          | 68.89        | 69.24          | 62.69        | 76.64          | 74.04        |
| ShuffleNet_SS | 73.30          | 71.12        | 73.62          | 70.23        | 71.55          | 69.17        | 70.21          | 68.73        | 68.52          | 68.36        | 69.89          | 63.17        | 76.87          | 73.32        |
| DLBLS_SS      | 73.35          | <b>71.96</b> | 73.95          | <b>72.07</b> | <b>71.65</b>   | <b>70.04</b> | <b>70.54</b>   | <b>69.34</b> | <b>68.59</b>   | <b>69.33</b> | <b>70.24</b>   | <b>63.58</b> | 77.35          | <b>75.08</b> |

because the powerful analytical ability and broad receptive field of DLBLS\_SS can effectively capture the key local and long-range dependencies in high-dimensional protein sequences, which can optimize the problem of insufficient feature extraction and enhance the ability of secondary structure recognition. Furthermore, we performed a paired *t*-test<sup>47</sup> on the Q<sub>8</sub> accuracy of each protein of these models on the CB513 dataset with a confidence level of 0.05. In the *t*-test, there are significant differences between DLBLS\_SS and the other five state-of-the-art models. Among them, our model is the closest to the mean of ShuffleNet\_SS.

## 4 Conclusions

In this paper, we combine deep learning and BLS to propose a novel model DLBLS\_SS for 3-state and 8-state PSSP. In DLBLS\_SS, the BLSTM module can extract global features in protein sequences, the SEBTCN module can bidirectionally capture key deep long-range dependencies in residue sequences, and the BLS module can further capture local interactions between residues while rapidly optimizing the extracted features. SEBTCN is our proposed sequence-to-sequence prediction network based on TCN and channel attention mechanism. We test the prediction performance of the proposed DLBLS\_SS on the public test sets CASP10, CASP11, CASP12, CASP13, CASP14 and CB513 using the evaluation metrics Q<sub>3</sub> accuracy, Q<sub>8</sub> accuracy and SOV score. Experimental results show that the proposed DLBLS\_SS exhibits state-of-the-art prediction performance compared to five popular models. The proposed model has powerful feature extraction ability, which can comprehensively utilize local and global optimal features for prediction to improve secondary structure recognition. In the future, we will

continue to study techniques such as feature extraction and fusion in PSSP while exploring complex sequence–structure relationships.

## Data availability

The dataset and code for this study are at [https://github.com/yuanlu9707/DLBLS\\_SS](https://github.com/yuanlu9707/DLBLS_SS).

## Author contributions

LY, XH, YM and YL conceived the idea for this research. LY and XH implement the model. LY, XH and YM collected the data. LY and YM wrote the manuscript, YM and YL supervised the research and reviewed the manuscript. All authors contributed to the article and approved the submitted version.

## Conflicts of interest

There are no conflicts to declare.

## Acknowledgements

This work was supported by the National Natural Science Foundation of China [grant number 61375013] and the Natural Science Foundation of Shandong Province [grant number ZR2013FM020].

## Notes and references

- 1 Y. Yang, J. Gao, J. Wang, R. Heffernan, J. Hanson, K. Paliwal and Y. Zhou, *Briefings Bioinf.*, 2018, **19**, 482–494.



- 2 P. Kumar, S. Bankapur and N. Patil, *Appl. Soft Comput.*, 2020, **86**, 105926.
- 3 Y. Wang, H. Mao and Z. Yi, *Knowl.-Based Syst.*, 2017, **118**, 115–123.
- 4 G. Wang, Y. Zhao and D. Wang, *Neurocomputing*, 2008, **72**, 262–268.
- 5 W. Kabsch and C. Sander, *Biopolymers*, 1983, **22**, 2577–2637.
- 6 A. Yaseen and Y. Li, *BMC Bioinf.*, 2014, **15**, 1–8.
- 7 Y. Ma, Y. Liu and J. Cheng, *Sci. Rep.*, 2018, **8**, 1–10.
- 8 S. Hua and Z. Sun, *J. Mol. Biol.*, 2001, **308**, 397–407.
- 9 B. Yang, Q. Wu, Z. Ying and H. Sui, *Knowl.-Based Syst.*, 2011, **24**, 304–313.
- 10 S. Salzberg and S. Cost, *J. Mol. Biol.*, 1992, **227**, 371–374.
- 11 R. Bondugula, O. Duzlevski and D. Xu, *Profiles and fuzzy k-nearest neighbour algorithm for protein secondary structure prediction*, 2005.
- 12 N. Qian and T. J. Sejnowski, *J. Mol. Biol.*, 1988, **202**, 865–884.
- 13 E. Faraggi, T. Zhang, Y. Yang, L. Kurgan and Y. Zhou, *J. Comput. Chem.*, 2012, **33**, 259–267.
- 14 L. J. McGuffin, K. Bryson and D. T. Jones, *Bioinformatics*, 2000, **16**, 404–405.
- 15 A. Drozdetskiy, C. Cole, J. Procter and G. J. Barton, *Nucleic Acids Res.*, 2015, **43**, W389–W394.
- 16 C. N. Magnan and P. Baldi, *Bioinformatics*, 2014, **30**, 2592–2597.
- 17 S. Wang, J. Peng, J. Ma and J. J. Xu, *Sci. Rep.*, 2016, **6**, 1–11.
- 18 J. Zhou and O. Troyanskaya, *Deep supervised and convolutional generative stochastic network for protein secondary structure prediction*, 2014.
- 19 R. Heffernan, Y. Yang, K. Paliwal and Y. Zhou, *Bioinformatics*, 2017, **33**, 2842–2849.
- 20 J. Hanson, K. Paliwal, T. Litfin, Y. Yang and Y. Zhou, *Bioinformatics*, 2019, **35**, 2403–2410.
- 21 M. S. Klausen, M. C. Jespersen, H. Nielsen, K. K. Jensen, V. I. Jurtz, C. K. Soenderby, M. O. A. Sommer, O. Winther, M. Nielsen and B. Petersen, *Proteins: Struct., Funct., Bioinf.*, 2019, **87**, 520–527.
- 22 M. R. Uddin, S. Mahbub, M. S. Rahman and M. S. Bayzid, *Bioinformatics*, 2020, **36**, 4599–4608.
- 23 G. Xu, Q. Wang and J. Ma, *Bioinformatics*, 2020, **36**, 5021–5026.
- 24 Z. Lyu, Z. Wang, F. Luo, J. Shuai and Y. Huang, *Front. Bioeng. Biotechnol.*, 2021, 404.
- 25 J. Hu, L. Shen and G. Sun, *Squeeze-and-excitation networks*, 2018.
- 26 S. Bai, J. Z. Kolter and V. J. Koltun, *An empirical evaluation of generic convolutional and recurrent networks for sequence modeling*, 2018.
- 27 A. Graves and J. Schmidhuber, *Neural Networks*, 2005, **18**, 602–610.
- 28 C. P. Chen and Z. Liu, *IEEE Trans. Neural Networks Learn. Syst.*, 2017, **29**, 10–24.
- 29 D. T. Jones, *J. Mol. Biol.*, 1999, **292**, 195–202.
- 30 M. Schuster and K. K. Paliwal, *IEEE Trans. Signal Process.*, 1997, **45**, 2673–2681.
- 31 S. Hochreiter and J. Schmidhuber, *Neural Comput.*, 1997, **9**, 1735–1780.
- 32 Y.-H. Pao and Y. Takefuji, *IEEE Comput.*, 1992, **25**, 76–79.
- 33 G. Wang and R. L. Dunbrack, *Nucleic Acids Res.*, 2005, **33**, W94–W98.
- 34 J. Moulton, K. Fidelis, A. Kryshtafovych, T. Schwede and A. Tramontano, *Proteins: Struct., Funct., Bioinf.*, 2014, **82**, 1–6.
- 35 J. Moulton, K. Fidelis, A. Kryshtafovych, T. Schwede and A. Tramontano, *Proteins: Struct., Funct., Bioinf.*, 2016, **84**, 4–14.
- 36 J. Moulton, K. Fidelis, A. Kryshtafovych, T. Schwede and A. J. P. S. Tramontano, *Proteins: Struct., Funct., Bioinf.*, 2018, **86**, 7–15.
- 37 A. Kryshtafovych, T. Schwede, M. Topf, K. Fidelis and J. Moulton, *Proteins: Struct., Funct., Bioinf.*, 2019, **87**, 1011–1020.
- 38 A. Kryshtafovych, T. Schwede, M. Topf, K. Fidelis and J. Moulton, *Proteins: Struct., Funct., Bioinf.*, 2021, **89**, 1607–1617.
- 39 J. A. Cuff and G. Barton, *Proteins: Struct., Funct., Bioinf.*, 1999, **34**, 508–519.
- 40 S. F. Altschul, T. L. Madden, A. A. Schäffer, J. Zhang, Z. Zhang, W. Miller and D. J. Lipman, *Nucleic Acids Res.*, 1997, **25**, 3389–3402.
- 41 A. Zemla, Č. Venclovas, K. Fidelis and B. Rost, *Proteins: Struct., Funct., Bioinf.*, 1999, **34**, 220–223.
- 42 Z. Li and Y. J. Yu, *Protein secondary structure prediction using cascaded convolutional and recurrent neural networks*, 2016.
- 43 I. Drori, I. Dwivedi, P. Shrestha, J. Wan, Y. Wang, Y. He, A. Mazza, H. Krogh-Freeman, D. Leggas and K. J. Sandridge, *High quality prediction of protein q8 secondary structure by diverse neural network architectures*, 2018.
- 44 Y. Guo, W. Li, B. Wang, H. Liu and D. Zhou, *BMC Bioinf.*, 2019, **20**, 1–12.
- 45 C. Fang, Y. Shang and D. Xu, *Proteins: Struct., Funct., Bioinf.*, 2018, **86**, 592–598.
- 46 W. Yang, Z. Hu, L. Zhou and Y. J. Jin, *Knowl.-Based Syst.*, 2022, **237**, 107771.
- 47 H. Hsu and P. A. Lachenbruch, *Paired t test*, 2014.

